Nuclear momentum distributions governed by Rabi flopping in the dissociation of hydrogen molecular ions in strong laser fields

Chen-Xi Hu[1] and Feng He [1,2,*]

[1]*Key Laboratory for Laser Plasmas (Ministry of Education) and School of Physics and Astronomy,*
Collaborative Innovation Center for IFSA (CICIFSA), Shanghai Jiao Tong University, Shanghai 200240, China
[2]*CAS Center for Excellence in Ultra-intense Laser Science, Shanghai 201800, China*

We study the Rabi flopping between the $1s\sigma_g$ and $2p\sigma_u$ states during the dissociation of hydrogen molecular ions in strong laser fields by numerically simulating the time-dependent Schrödinger equation. Starting either from a certain vibrational state or from coherently superimposed vibrational states weighted with Frank-Condon factors, the dissociative nuclear momentum distributions present multiple angular nodes and maxima due to molecular alignment-dependent Rabi flopping. The Rabi frequency and nuclear angular distribution depend on the laser chirp and laser ellipticity. Rabi flopping also determines the population on the $2p\sigma_u$ state and thus the dissociation probability. The deep understanding of Rabi flopping in molecular dissociation gives clues to control ultrafast molecular dynamics.

I. INTRODUCTION

Exposed to strong laser fields, molecules may absorb photons and undergo complex reactions. One of the typical molecular reactions is dissociation [1], in which the electron absorbs energy and jumps to an excited state, followed by the nuclei-nuclei repulsion. Finally, one molecule breaks into several fragments. Experimentally, by measuring the momenta of fragments, one may retrieve the dissociation pathways and extract the mechanisms governing molecular reactions [2–4]. Due to its simplicity, the hydrogen molecular ion has been studied extensively both theoretically and experimentally. It is now clear that the laser coupling between the two lowest electronic states $1s\sigma_g$ and $2p\sigma_u$ mainly governs the dissociation process [5]. For example, the electron may absorb one photon and dissociate along the $2p\sigma_u$ state. Such a one-photon transition mainly happens at the internuclear distance R_c where the energy difference between the $1s\sigma_g$ and $2p\sigma_u$ states equates to the photon energy, as shown in Fig. 1 by the red arrow. If the laser field is stronger, the electron may absorb three photons simultaneously at a small internuclear distance $R_{3\omega}$, followed by the emission of one photon at a large internuclear distance R_c, as shown in Fig. 1 by the blue arrows. However, if the laser pulse is very short, the later one-photon emission may not happen. These typical pathways are termed one-photon [6,7], three-photon [8,9], and net-two-photon [10] dissociation. For a complex molecule with more than one electron, some other dissociation pathways may happen, mediated by the electron-electron correlation [11,12]. Experimentally, several dissociation pathways may coexist, and the coexistence of different dissociation pathways may interfere and induce some interesting scenarios. If the molecule dissociates

via one-photon and net-two-photon pathways having opposite parities, the interference of these two states leads to the asymmetric electron localization on two nuclei. The electron localization can be controlled by many different strategies [13–29]. In contrast, if two pathways with the same parity, such as one-photon and three-photon pathways, are initiated by a circularly polarized laser pulse, the proton angular distributions show some vorticose structures [30,31].

Rabi flopping is a universal scenario in the quantum world. Though Rabi flopping in atoms has been extensively covered in the literature [32], Rabi flopping in molecules has seldom been studied. Since the dissociation of H_2^+ is mostly determined by the laser coupling between the $1s\sigma_g$ and $2p\sigma_u$ states, one expects to see the Rabi flopping in such a two-level quantum system [33]. The Rabi flopping in molecules is distinct from that in atoms in several aspects. In atoms, the energy difference between the two related states remains constant and thus the Rabi frequency in an atom is constant once a laser is given. However, in molecular dissociation, the energy difference between the two electronic states depends on the internuclear distance and thus the timing of the molecular stretching. One may expect that the Rabi frequency is varying during the molecular dissociation. On the other hand, atoms are isotropic in space and thus no alignment needs to be considered. In molecular dissociation, the transition dipole is along the molecular axis and the laser-molecule coupling depends on the molecular alignment. Angle-resolved Rabi flopping was recently observed in simulation [33].

Angle-resolved Rabi flopping determines the proton angular distribution in the dissociation of H_2^+. Since the angular distribution of dissociation fragments is used to retrieve molecular dynamics in many studies, it is necessary to investigate how laser parameters modify Rabi flopping in molecular dissociation. Since chirp exists generally in few-cycle laser pulses, it is necessary to explore how this inherent

parameter modifies the molecular dissociation. Another important parameter is laser ellipticity, which can be accurately tuned experimentally. In this paper, we systematically simulate how the laser chirp and ellipticity modify the angle-resolved Rabi flopping in the dissociation of H_2^+ in strong laser fields. The rest of the paper is organized as followed. In Sec. II we introduce the details of our numerical method. Section III presents the simulation results. The paper ends with a summary in Sec. IV.

II. NUMERICAL METHODS

For H_2^+, the potential curves of the $1s\sigma_g$ and $2p\sigma_u$ states are far away from other potential curves, and the photon coupling between the $1s\sigma_g$ and $2p\sigma_u$ states is much stronger than others. Therefore, the dissociation of H_2^+ in strong laser fields can be simulated using the two-level numerical model [34] (atomic units are used unless stated otherwise)

$$
i\frac{\partial}{\partial t}\begin{pmatrix}\chi_g(\mathbf{R},t)\\\chi_u(\mathbf{R},t)\end{pmatrix}
$$
$$
=\begin{pmatrix}\frac{\mathbf{P_R}^2}{2M}+V_g(\mathbf{R}) & \mathbf{D}(\mathbf{R})\cdot\mathbf{E}(t)\\ \mathbf{D}(\mathbf{R})\cdot\mathbf{E}(t) & \frac{\mathbf{P_R}^2}{2M}+V_u(\mathbf{R})\end{pmatrix}\begin{pmatrix}\chi_g(\mathbf{R},t)\\\chi_u(\mathbf{R},t)\end{pmatrix}, \quad (1)
$$

where $\mathbf{R}$ encodes the internuclear distance and molecular alignment, $\mathbf{D}(\mathbf{R})$ is the $\mathbf{R}$-dependent dipole between two electronic states [35], $\mathbf{D}(\mathbf{R})=\langle\phi_g|\mathbf{r}|\phi_u\rangle$, M is the reduced nuclear mass, and $V_g(\mathbf{R})$ and $V_u(\mathbf{R})$ are the potential surfaces for H_2^+ in $1s\sigma_g$ and $2p\sigma_u$ states, respectively [35]. The potential surfaces can be obtained by $V_{g(u)}(\mathbf{R})=\frac{1}{|\mathbf{R}|}+\langle\phi_{g(u)}|-\frac{\nabla_{\mathbf{r}}^2}{2}+V(\mathbf{r},\mathbf{R})|\phi_{g(u)}\rangle$. Here $\mathbf{P_R}=-i\nabla_{\mathbf{R}}=-i(\hat{x}\frac{\partial}{\partial R_x}+\hat{y}\frac{\partial}{\partial R_y})$ is the nuclear momentum operator and $\mathbf{E}(t)$ is the electric field of the laser pulse. For simplicity, we confine $\mathbf{R}$ in the plane constructed by the molecular axis and laser polarization. This approximation is reasonable since no important dynamics occurs in the direction perpendicular to this plane. Here χ_g and χ_u are the nuclear wave packets of H_2^+ associated with electrons in $1s\sigma_g$ and $2p\sigma_u$ states, respectively. In this model, the nuclear rotation is already included. The spatial grids are $0 < R_x < 30$ a.u. and $0 < R_y < 30$ a.u. and the spatial steps are $dR_x = dR_y = 0.02$ a.u. The simulation box is big enough to hold all dissociative wave packets during the interaction and thereby no absorbing boundary conditions are used, which has been verified by test calculations using or omitting absorbing boundaries. The converged results have been obtained by using the time step $dt = 0.1$ a.u. Initially, $\chi_u(\mathbf{R}, t=0) = 0$ and $\chi_g(\mathbf{R}, t=0)$ depends on the concrete physical situations. For example, in the case of photoionization of H_2 in laser fields, the acquired nuclear wave packet of H_2^+ is in the coherent superposition of a series of vibrational states. Usually, the Frank-Condon approximation is adopted for such a case and thus $\chi_g(\mathbf{R}, t=0) = \chi_{H_2}$, where χ_{H_2} is the nuclear ground state of H_2 and has an almost isotropic distribution in space. In the case of the dissociation of the H_2^+ ion beam produced from a low-energy ion accelerator [2,3,36], the nuclear wave packet of H_2^+ may be incoherent. Thereby, the numerical simulations may start from different vibrational states of H_2^+ separately [23]. In the following simulations, we will start either from a certain vibrational state or from a coherent
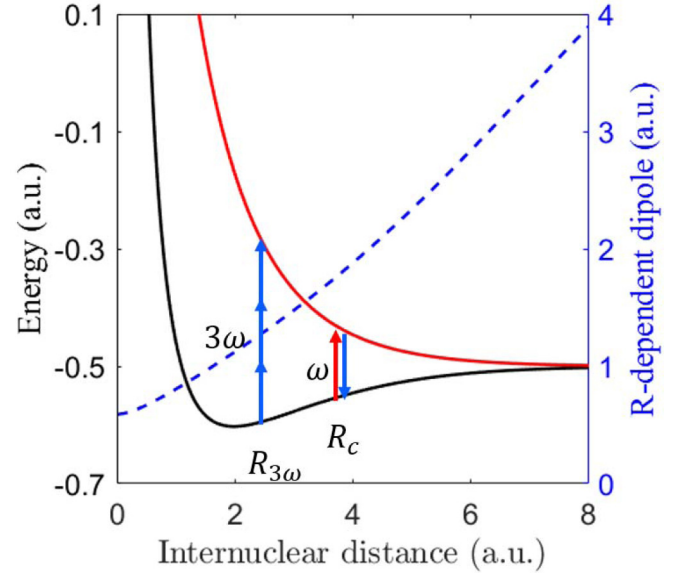

FIG. 1. Potential curves of the $1s\sigma_g$ (black solid curve) and $2p\sigma_u$ (red solid curve) states of H_2^+. The red arrow represents the one-photon transition. The blue arrows indicate the three-photon absorption followed by one-photon emission. The blue dashed line represents the R-dependent transition dipole between the $1s\sigma_g$ and $2p\sigma_u$ states.

supposition of several vibrational states. The initial states are numerically obtained by the imaginary-time propagation algorithm [37]. We propagate Eq. (1) using the Crank-Nicolson method [38]. After the laser-H_2^+ interaction, we keep propagating the wave packet until the dissociative nuclear wave packet enters the area $|\mathbf{R}| > 10$ and clearly separates from the bound states. By Fourier transforming the dissociative nuclear wave packet, we obtain the nuclear wave packet in momentum representation, from which the momentum distribution and energy spectrum can be built.

III. RESULTS

We first study the nuclear momentum distribution induced by a few-cycle laser field

$$
\mathbf{E}(t) = E_0 \cos(\omega_0 t)\sin^2\left(\frac{\pi t}{\tau}\right)\hat{x}, \quad 0 < t < \tau. \quad (2)
$$

The laser parameters are $E_0 = 0.0534$ a.u. (the corresponding laser intensity is 10^{14} W/cm^2), the frequency $\omega_0 = 0.114$ (400 nm), and the pulse duration $\tau = 8$ fs (six optical cycles). For a driving laser pulse with a wavelength of 400 nm, the resonant one-photon transition happens at the internuclear distance $R_c = 3.8$ a.u. Figures 2(a) and 2(b) show the nuclear momentum distributions of the dissociation of H_2^+ and D_2^+, respectively. The angular distributions are shown in Fig. 2(c). One vibrational state is initially adopted in the simulations. From left to right, the vibrational states $v = 4$–9 are used, respectively. Overall, the momenta in Fig. 2(b) are $\sqrt{2}$ times those in Fig. 2(a) and the kinetic energies in each column are almost the same. As explained in [33], the laser-H_2^+ interaction may form the Rabi flopping between the $1s\sigma_g$ and $2p\sigma_u$ states, and this Rabi frequency depends
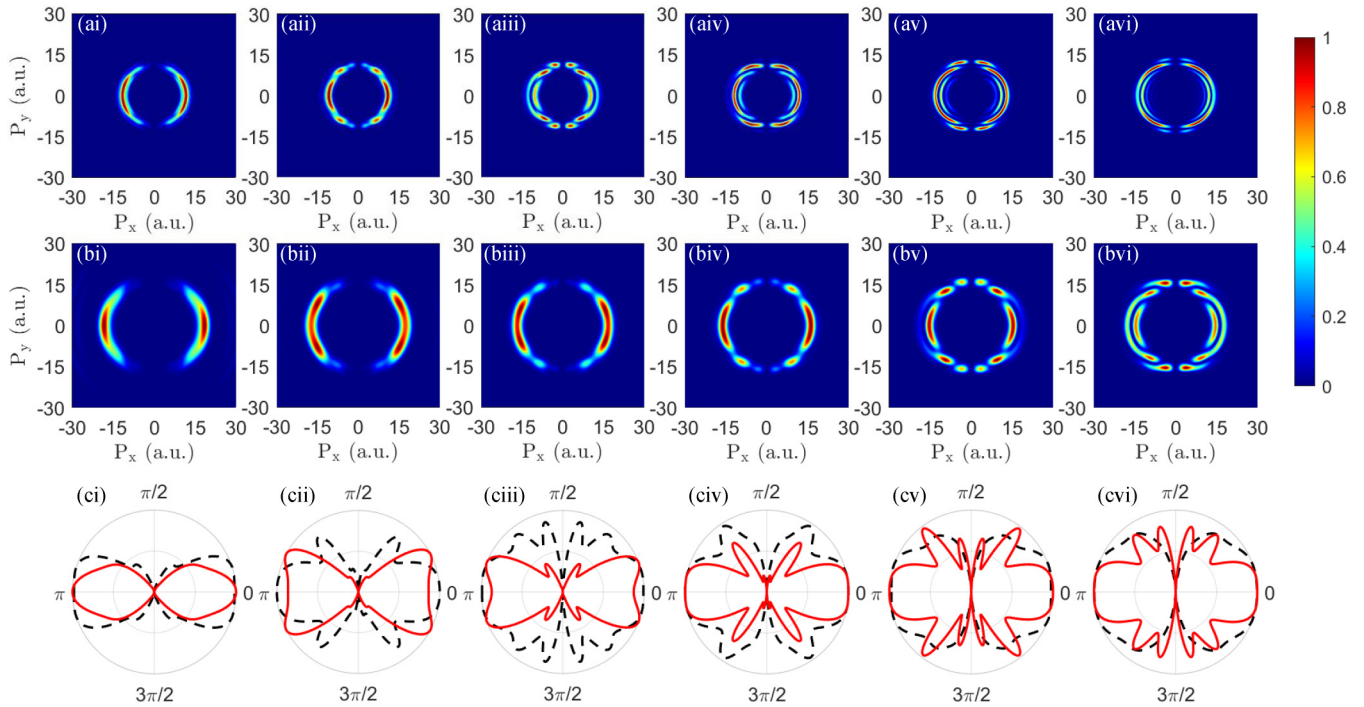
FIG. 2. Nuclear momentum distributions after the dissociation of (a) H_2^+ and (b) D_2^+. (c) Nuclear angular distributions for the dissociation of H_2^+ (black dashed line) and D_2^+ (red solid line) for dissociation starting from the vibrational states (i) $v = 4$, (ii) $v = 5$, (iii) $v = 6$, (iv) $v = 7$, (v) $v = 8$, and (vi) $v = 9$. The laser parameters are an intensity of 1×10^{14} W/cm^2, wavelength of 400 nm, and duration of six optical cycles (8 fs). All plots here are normalized to their maximum values. The dissociation rates of H_2^+ from the vibrational states $v = 4$–9 are 0.1345, 0.2931, 0.3676, 0.3333, 0.3078, and 0.2828, respectively. The dissociation rates of D_2^+ from the vibrational states $v = 4$–9 are 0.0191, 0.1010, 0.2144, 0.2372, 0.1878, and 0.1644, respectively.

on the molecular orientation direction. Here one may clearly see that the Rabi flopping depends sensitively on the vibrational states. For the low vibrational states, such as the $v = 4$ state used in Figs. 2(a i) and 2(b i), the initially nuclear wave packets are distributed in the area with an internuclear distance smaller than $R_c = 3.8$ a.u. and thus the one-photon resonant transition is too faint to initiate the Rabi flopping. For high vibrational states such as $v = 7$–9, there are enough populations at around $R_c = 3.8$ a.u. and the resonant photon coupling triggers strong Rabi flopping, producing multiple minima and maxima in the angular distributions [33]. Figures 2(a ii) and 2(b iv), Figs. 2(a iii) and 2(b v), and Figs. 2(a iv) and 2(b vi) are similar to each other. This is due to their similar initial nuclear wave-packet distribution at around $R_c = 3.8$ a.u. Besides the angular structures induced by Rabi flopping, Figs. 2(a vi) and 2(b vi) also show concentric rings (or multiple peaks in the direction $\theta = 0$). This is due to the initial distribution of vibrational states, which have several radial nodes and maxima at around the internuclear distance R_c.

In the photoionization of H_2, the created nuclear wave packets are superimposed vibrational states weighted by the Frank-Condon factors [39]. Starting from such superimposed coherent states, the biggest difference from the previous case is that the molecular bond stretches and then shrinks alternatively. In the following, we investigate the Rabi flopping in such a vibrating molecule. To look at how the nuclear movement affects the Rabi flopping, we introduce the chirped

laser pulse in the calculations

$$\mathbf{E}(t) = E_0 \cos[\omega(t - t_0)] \sin^2\left(\frac{\pi(t - t_0)}{\tau}\right)\hat{x}, \quad t_0 < t < \tau + t_0,$$

(3)

where t_0 is free propagation time and $\omega = \omega_0 + \xi(t - t_0 - \tau/2)$ is the time-dependent frequency of the chirped laser pulse. Here ξ is the coefficient describing the rate of frequency change; $\xi > 0$ and $\xi < 0$ correspond to positive and negative chirps, i.e., the laser frequency increases or decreases with time, respectively. The laser intensity is 5×10^{13} W/cm^2 and the other laser parameters are the same as those used in Fig. 2. The laser pulses with positive and negative chirps are presented in Fig. 3(e). We first freely propagate the nuclear wave packet for $t_0 = 8$ fs, and thus the nuclear wave packet is mainly distributed in the range $3 < R < 8$ a.u., assisting the one-photon transition. Figures 3(b), 3(c), and 3(d) show the nuclear momentum distributions induced by negatively chirped, nonchirped, and positively chirped laser pulses, respectively. The observed angle-resolved structures have been explained by the angle-dependent Rabi flopping between the $1s\sigma_g$ and $2p\sigma_u$ states [33]. Though the laser electric fields in Fig. 3(e) look similar, the nuclear momentum distributions in Figs. 3(b) and 3(d) are distinct. It is clear that the nuclear momentum distribution initiated by the negatively chirped laser pulse has multiple nodes and maxima at different angles and has a minimum along the laser polarization. However,
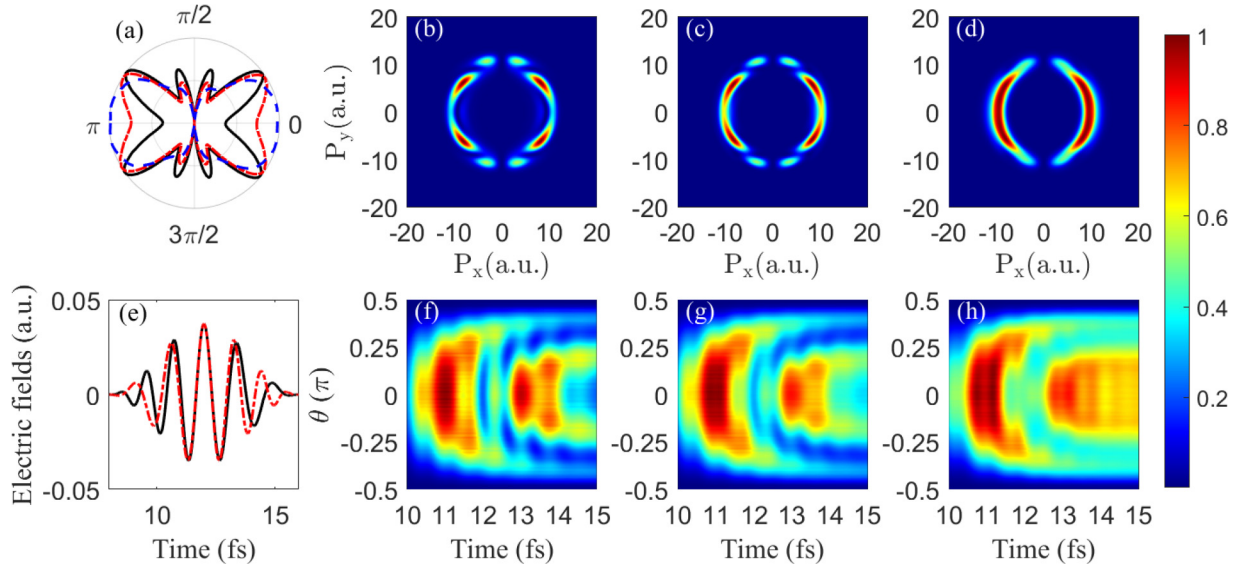
FIG. 3. (b)–(d) Nuclear momentum distributions and (f)–(h) time-revolved angular distributions, with (b) and (f) $\xi = -10^{-4}$, (c) and (g) $\xi = 0$, and (d) and (h) $\xi = 10^{-4}$. The laser intensity is 5×10^{13} W/cm^2 and the pulse duration is six optical cycles (8 fs). The central wavelength is 400 nm with $\omega_0 = 0.114$ a.u. The laser pulses begin at $t_0 = 8$ fs. (a) Nuclear momentum angular distributions induced by negatively chirped (black solid line), nonchirped (red dotted line), and positively chirped (blue dashed line) laser pulses. (e) Negatively chirped (black solid line) and positively chirped (red dotted line) laser electric fields. All plots here are normalized to their maximum values.

the nuclear momentum distribution induced by the positively chirped laser has fewer nodes. Figure 3(a) shows the nuclear angular distributions, obtained by radially integrating the momentum distributions in Figs. 3(b)–(d).

The theory of Rabi flopping is helpful to understand the striking difference in Figs. 3(b) and 3(d). In the simplified analytical Rabi model, the Rabi frequency is written as [32]

$$\omega_r = \sqrt{[V_u(R) - V_g(R) - \omega]^2 + [E_0 D(R) \cos\theta]^2}. \quad (4)$$

The photon absorption is most efficient at the internuclear distance where the two-level energy difference is the same as the photon energy. The central part of the laser pulse has H_2^+ acting mainly in the time interval 10–14 fs. During this period, the molecular bond is shrinking and the energy difference $V_u(R) - V_g(R)$ is increasing. However, the frequency of the negatively chirped laser pulse keeps decreasing. Such a mismatch makes ω_r large, resulting in the fast Rabi flopping. In contrast, the increasing frequency of the positively chirped pulse matches the increase of the energy difference $V_u(\mathbf{R}) - V_g(\mathbf{R})$ during the whole interaction time. Therefore, $V_u(R) - V_g(R) - \omega$ tends to be zero during the interaction and a slower Rabi flopping is activated. The time-resolved angular distributions shown in Figs. 3(f) and 3(h) clearly depict this difference. For example, in Fig. 3(f), in the direction $\theta = 0$, two complete Rabi oscillations are accomplished, leading to a minimum indicated by the black solid curve in Fig. 3(a). However, in Fig. 3(h), about 1.5 Rabi oscillations are finished at the end of the laser pulse in the direction $\theta = 0$. After the laser interaction, the large population on the $2p\sigma_u$ state contributes to the peak shown by the blue dashed line in Fig. 3(a). The case without chirps presents the scenario between the negative and the positive chirp, as shown in Figs. 3(c) and 3(g) and by the red dash-dotted line in Fig. 3(a).

The number of Rabi oscillations determines the population on the $2p\sigma_u$ state and thus the dissociation probability. Figures 4(a) and 4(b) show the dissociation probabilities as a function of the free propagation time before the laser is introduced. When the laser intensity is as weak as 10^{12} W/cm^2, no Rabi flopping is activated. Not surprisingly, both the negatively and the positively chirped pulses result in the same dissociation probability, as shown in Fig. 4(a). Due to the nuclear wave-function expansion, the local probability at the internuclear distance R_c is smaller if the free propagation time is longer. This explains the homogeneous decrease of the dissociation probability in Fig. 4(a). When the laser is intense enough to trigger Rabi flopping, the two chirped pulses result in different dissociation probabilities, as shown in Fig. 4(b). As explained above, the Rabi frequency depends on the chirp of the laser pulse and how the $2p\sigma_u$-$1s\sigma_g$ energy gap changes. If the free propagation time is small, say, 4 fs, the $2p\sigma_u$-$1s\sigma_g$ energy gap keeps decreasing when the laser pulse is acting on H_2^+. The variation tendency of the energy gap and the frequency of the negatively chirped laser pulse match each other, making the Rabi frequency smaller. However, if the free propagation time is so long that the internuclear distance gets smaller when the laser field acts on it, the negatively chirped laser pulse induces a larger Rabi frequency. Generally, a larger dissociation probability is formed if a half-integral Rabi oscillation is accomplished at the end of the laser pulse. However, also note that the Rabi frequencies are different for molecules aligned at different angles and the dissociation probability is the integration of all dissociative fragments at different angles. Hence, it is hard to say the dissociation probability monotonically depends on the Rabi frequency.

Besides the chirp of laser pulses, the laser ellipticity also plays an important role in Rabi flopping and the nuclear momentum distribution. For a linearly polarized laser pulse along the x axis, the effective laser intensity experienced by
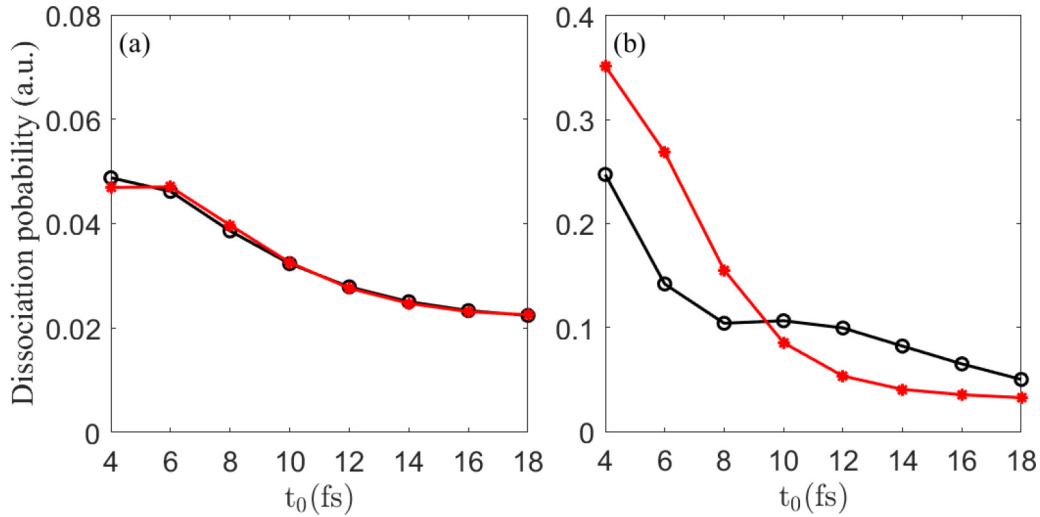
FIG. 4. Dissociation probabilities as a function of the free propagation time, with laser intensities of (a) 1×10^{12} W/cm^2 and (b) 5×10^{13} W/cm^2. The black lines with open circles and red lines with closed circles are calculated results using the negatively and positively chirped laser pulses, respectively. The other laser parameters are the same as those in Fig. 3.

the molecule aligned at θ is $E_0^2 \cos^2 \theta$. Such an effective laser intensity is completely changed if an elliptically polarized laser pulse is used. Hence, one may expect that the nuclear momentum distribution depends sensitively on the ellipticity. We take the same initial state as that used in Fig. 3 and freely propagate the nuclear wave packet for $t_0 = 8$ fs. Then the following elliptically polarized laser field is introduced:

$$\mathbf{E}(t) = E_0 \left[\frac{1}{\sqrt{1 + \varepsilon^2}} \cos(\omega_0 t) \hat{x} - \frac{\varepsilon}{\sqrt{1 + \varepsilon^2}} \sin(\omega_0 t) \hat{y} \right]$$
$$\times \sin^2 \left(\frac{\pi (t - t_0)}{\tau} \right), \quad t_0 < t < \tau + t_0. \quad (5)$$

Figures 5(a)–5(f) show the proton momentum distributions when the laser ellipticities are 0, 0.2, 0.4, 0.6, 0.8, and 1, respectively. Compared to Fig. 5(a), where the linearly polarized laser pulse is used, the maxima and nodes in momentum distribution change significantly with the change of laser

ellipticities. With a larger ellipticity, fewer angular nodes are obtained. It is intuitive that the rotational symmetry for the nuclear momentum distribution is presented when a circularly polarized laser field is used. When the ellipticity is 0.8, counterintuitively, the main dissociative fragments propagate in the $\hat{y}$ direction, along which the laser electric field is weak, and very few fragments propagate along the main axis of the driving laser field. Since an elliptically polarized laser pulse can be divided into two linearly polarized laser pulses, the mechanism can be understood similar to the case of a linearly polarized pulse. When the ellipticity is 0.8, the dissociative fragments propagating in the $\hat{y}$ direction experience lower effective laser intensity and fewer Rabi cycles than those in the $\hat{x}$ direction, resulting in more dissociative fragments in the $\hat{y}$ direction. One may expect that the nuclear momentum distribution can be modulated significantly by changing the ellipticity of laser pulses.

IV. CONCLUSION

In summary, laser pulses initiate angle-dependent Rabi flopping during molecular dissociation. By accomplishing different numbers of Rabi oscillations between the $1s\sigma_g$ and $2p\sigma_u$ states, the electron may have large or small populations on the $2p\sigma_u$ state at different angles, leading to angular nodes and maxima in the dissociative nuclear momentum distributions. Positively and negatively chirped laser pulses result in different dissociation probabilities if they are strong enough to activate the Rabi flopping. The angle-dependent Rabi flopping can be sensitively modified by the laser ellipticity. Depending on the laser intensity and pulse duration, an elliptically polarized pulse may induce more dissociative fragments along its short elliptical axis than along its long elliptical axis. Looking forward, using the pump-probe scheme, the pump pulse induced angle-dependent dissociation may be followed by angle-dependent ionization by the probe pulse.
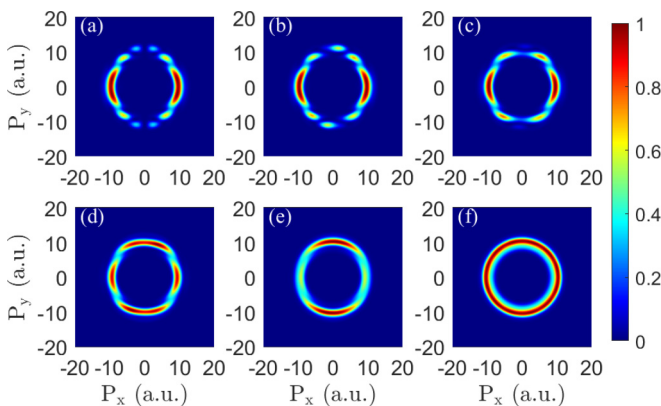

FIG. 5. Proton momentum distributions when the laser ellipticity is (a) 0, (b) 0.2, (c) 0.4, (d) 0.6, (e) 0.8, and (f) 1.0. The laser intensity is 1×10^{14} W/cm^2. All other parameters are the same as in Fig. 2. All plots here are normalized to their maximum values.

[1] S. Chelkowski, T. Zuo, O. Atabek, and A. D. Bandrauk, Phys. Rev. A **52**, R2511 (1995).

[2] K. Sändig, H. Figger, and T. W. Hänsch, Phys. Rev. Lett. **85**, 4876 (2000).

[3] I. Ben-Itzhak, P. Q. Wang, J. F. Xia, A. M. Sayler, M. A. Smith, K. D. Carnes, and B. D. Esry, Phys. Rev. Lett. **95**, 073002 (2005).

[4] P. Lu, W. Zhang, X. Gong, Q. Song, K. Lin, Q. Ji, J. Ma, F. He, H. Zeng, and J. Wu, Phys. Rev. A **95**, 033404 (2017).

[5] A. Giusti-Suzor, F. H. Mies, L. F. DiMauro, E. Charron, and B. Yang, J. Phys. B **28**, 309 (1995).

[6] P. H. Bucksbaum, A. Zavriyev, H. G. Muller, and D. W. Schumacher, Phys. Rev. Lett. **64**, 1883 (1990).

[7] A. D. Bandrauk and M. L. Sink, J. Chem. Phys. **74**, 1110 (1981).

[8] A. Giusti-Suzor and F. H. Mies, Phys. Rev. Lett. **68**, 3869 (1992).

[9] J. McKenna, F. Anis, A. M. Sayler, B. Gaire, N. G. Johnson, E. Parke, K. D. Carnes, B. D. Esry, and I. Ben-Itzhak, Phys. Rev. A **85**, 023405 (2012).

[10] A. Giusti-Suzor, X. He, O. Atabek, and F. H. Mies, Phys. Rev. Lett. **64**, 515 (1990).

[11] M. F. Kling, C. Siedschlag, A. J. Verhoef, J. I. Khan, M. Schultze, T. Uphues, Y. Ni, M. Uiberacker, M. Drescher, F. Krausz, and M. J. J. Vrakking, Science **312**, 246 (2006).

[12] P. Lu, J. Wang, H. Li, K. Lin, X. Gong, Q. Song, Q. Ji, W. Zhang, J. Ma, H. Li, H. Zeng, F. He, and J. Wu, Proc. Natl. Acad. Sci. USA **115**, 2049 (2018).

[13] V. Roudnev, B. D. Esry, and I. Ben-Itzhak, Phys. Rev. Lett. **93**, 163601 (2004).

[14] V. Roudnev and B. D. Esry, Phys. Rev. Lett. **99**, 220406 (2007).

[15] F. He, C. Ruiz, and A. Becker, Phys. Rev. Lett. **99**, 083002 (2007).

[16] F. He, A. Becker, and U. Thumm, Phys. Rev. Lett. **101**, 213002 (2008).

[17] D. Ray, F. He, S. De, W. Cao, H. Mashiko, P. Ranitovic, K. P. Singh, I. Znakovskaya, U. Thumm, G. G. Paulus, M. F. Kling, I. V. Litvinyuk, and C. L. Cocke, Phys. Rev. Lett. **103**, 223201 (2009).

[18] M. Kremer, B. Fischer, B. Feuerstein, V. L. B. de Jesus, V. Sharma, C. Hofrichter, A. Rudenko, U. Thumm, C. D. Schröter, R. Moshammer, and J. Ullrich, Phys. Rev. Lett. **103**, 213003 (2009).

[19] F. Kelkensberg, C. Lefebvre, W. Siu, O. Ghafur, T. T. Nguyen-Dang, O. Atabek *et al.*, Phys. Rev. Lett. **103**, 123005 (2009).

[20] G. Sansone, F. Kelkensberg, J. F. P. Torres, F. Morales, M. F. Kling, W. Siu *et al.*, Nature (London) **465**, 763 (2010).

[21] B. Fischer, M. Kremer, T. Pfeifer, B. Feuerstein, V. Sharma, U. Thumm, C. D. Schröter, R. Moshammer, and J. Ullrich, Phys. Rev. Lett. **105**, 223001 (2010).

[22] K. P. Singh, F. He, P. Ranitovic, W. Cao, S. De, D. Ray, S. Chen, U. Thumm, A. Becker, M. M. Murnane, H. C. Kapteyn, I. V. Litvinyuk, and C. L. Cocke, Phys. Rev. Lett. **104**, 023001 (2010).

[23] F. Anis and B. D. Esry, Phys. Rev. Lett. **109**, 133001 (2012).

[24] I. Znakovskaya, P. von den Ho, G. Marcus, S. Zherebtsov, B. Bergues, X. Gu, Y. Deng, M. J. J. Vrakking, R. Kienberger, F. Krausz, R. de Vivie-Riedle, and M. F. Kling, Phys. Rev. Lett. **108**, 063002 (2012).

[25] A. González-Castrillo, A. Palacios, H. Bachau, and F. Martín, Phys. Rev. Lett. **108**, 063009 (2012).

[26] N. G. Kling, K. J. Betsch, M. Zohrabi, S. Zeng, F. Anis, U. Ablikim, B. Jochim, Z. Wang, M. Kübel, M. F. Kling, K. D. Carnes, B. D. Esry, and I. Ben-Itzhak, Phys. Rev. Lett. **111**, 163004 (2013).

[27] T. Rathje, A. M. Sayler, S. Zeng, P. Wustelt, H. Figger, B. D. Esry, and G. G. Paulus, Phys. Rev. Lett. **111**, 093002 (2013).

[28] X. Gong, P. He, Q. Song, Q. Ji, H. Pan, J. Ding, F. He, H. Zeng, and J. Wu, Phys. Rev. Lett. **113**, 203001 (2014).

[29] H. Xu, Z. Li, F. He, X. Wang, A. Atia-Tul-Noor, D. Kielpinski, R. T. Sang, and I. V. Litvinyuk, Nat. Commun. **8**, 15849 (2017).

[30] Z. Chen, P.-L. He, and F. He, Phys. Rev. A **101**, 033406 (2020).

[31] Z. Chen and F. He, Phys. Rev. A **102**, 033107 (2020).

[32] M. O. Scully and M. S. Zubairy, *Quantum Optics* (Cambridge University Press, Cambridge, 1997), pp. 151–154.

[33] C.-X. Hu, W.-Z. Li, W.-B. Zhang, X.-C. Gong, J. Wu, and F. He, Phys. Rev. A **103**, 043122 (2021).

[34] E. Charron, A. G. Suzor, and F. H. Mies, J. Chem. Phys. **103**, 7359 (1995).

[35] T. E. Sharp, At. Data Nucl. Data Tables **2**, 119 (1970).

[36] I. D. Williams, P. McKenna, B. Srigengan, I. M. G. Johnston, W. A. Bryan, J. H. Sanderson, A. El-Zein, T. R. J. Goodworth, W. R. Newell, P. F. Taday, and A. J. Langley, J. Phys. B **33**, 2743 (2000).

[37] R. Kosloff and H. Tal-ezer, Chem. Phys. Lett. **127**, 223 (1986).

[38] W. H. Press, S. A. Teukolsky, W. T. Vetterling, and B. P. Flannery, *Numerical Recipes: The Art of Scientific Computing*, 3rd ed. (Cambridge University Press, Cambridge, 2007), pp. 1048–1049.

[39] B. Feuerstein and U. Thumm, Phys. Rev. A **67**, 063408 (2003).